A biomechanical model for fluidization of cells under dynamic strain (Supporting Material)

Tenghu Wu

Department of Chemical and Biological Engineering,

University of British Columbia, Vancouver, BC V6T 1Z3, Canada

James J. Feng*

Department of Chemical and Biological Engineering,

University of British Columbia, Vancouver, BC V6T 1Z3, Canada, and

Department of Mathematics,

University of British Columbia, Vancouver, BC V6T 1Z2, Canada

Prior experiments have subjected adherent cells to different deformations, and recorded the critical strains and strain rates that are required for the disassembly of stress fibers (SFs) and fluidization of the cells. Thus it is interesting to explore the model predictions of these critical conditions, and compare them with experimental measurements. In our Kelvin-Voigt-Myosin (KVM) model, we will take the complete loss of tensile force in the SF, i.e. $\sigma = 0$, to be the critical condition. Such a choice is motivated by experimental observations that a stress fiber buckles and disintegrates after its pre-tension is relaxed by compression (1, 2, 3). It is also consistent with two microscopic effects. The first is the highly asymmetric load response of actin filaments: they can sustain considerable tension but buckle easily under pico-newtons of compression (4). The second is the enhanced detachment rate of myosin motors due to loss of tensile force (5, 6) (cf. Eq. 5 of the main text).

*Corresponding author. E-mail: james.feng@ubc.ca

1 Model predictions

Motivated by experimental data, we have chosen to construct a phase diagram in the strain–strain rate plane. Using the stretch-compress (SC) maneuver of Eq. (10), we carry out a series of simulations by varying either the total strain ε_0 or the strain rate $\dot{\varepsilon}_0$ while holding the other constant. As $\dot{\varepsilon}_0 = 2\varepsilon_0/T$, this is accomplished by adjusting the period T. The outcome is recorded as either fluidization or non-fluidization, depending on the sign of the minimum tension. The boundary between the two regimes is depicted in Fig. S1(a). Experimental observations suggest that fluidization occurs when either ε_0 or $\dot{\varepsilon}_0$ is high enough. Thus, one may have anticipated a sort of compensation between them, and a negative slope for the boundary in the $(\varepsilon_0, \dot{\varepsilon}_0)$ plane. The model shows, however, a non-monotonic boundary with a positive slope for large strain.

The key to understanding this behavior is to recognize that in our KVM model, the force σ in the SF is affected by the relaxation of the myosin apparatus. For a large strain ε_0, σ grows so much during the stretching phase (cf. Fig. 3a of the main text) that at its end ($t = T/2$), almost all the m_1 myosin motors have been converted to m_2 (cf. Fig. 4a). As a result, myosin walking and relaxation become negligible according to Eq. (6), and the myosin apparatus is essentially rigid. The subsequent compression, therefore, is sustained almost entirely by the Kelvin-Voigt (KV) element. In this regime, a larger ε_0 implies a larger elastic tension from the KV element at the end of stretch, which will protect the SF from disassembly during the subsequent compression. Thus, a faster strain rate $\dot{\varepsilon}_0$ is required for disassembly at larger strain ε_0, and the slope of the boundary should be positive. To be more precise, we estimate the minimum tension at the start of compression as $\sigma_{min} = GL_0(\varepsilon_p + \varepsilon_0) - \eta L_0 \dot{\varepsilon}_0$, where we have neglected the strain sustained by the myosin apparatus. Setting σ_{min} to zero then gives us a critical condition for fluidization that is a straight line of positive slope G/η in the $(\varepsilon_0, \dot{\varepsilon}_0)$ plane. This explains the right portion of Fig. S1(a); the actual slope of the boundary is 0.173 s^{-1}, reasonably close to the expected $G/\eta = 0.25\ \mathrm{s}^{-1}$. The difference is due to the sliding of the myosin motors. To rationalize the negative slope for small ε_0, we recognize that with decreasing ε_0, the myosin apparatus is more flexible with faster relaxation at the start of compression. Thus, the KV element will suffer less strain, and fluidization is achieved only with greater strain rate $\dot{\varepsilon}_0$. Hence the boundary takes on a negative slope at the left portion of Fig. S1(a). Incidentally, most prior

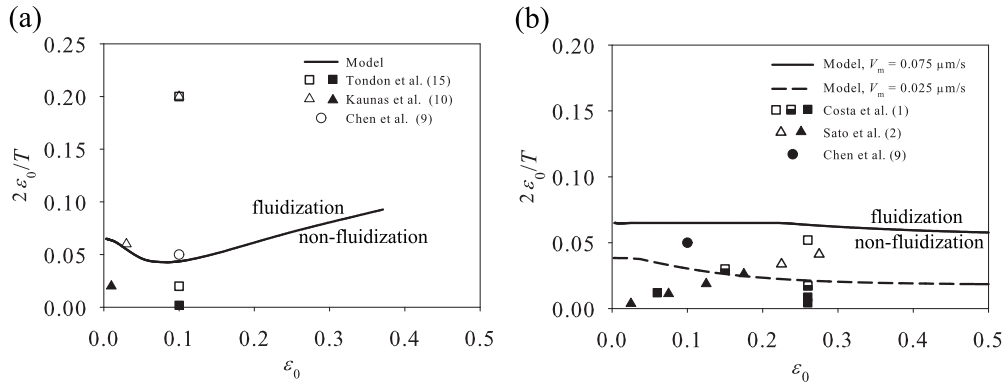

Figure S1: Critical conditions for SF disassembly depicted on the $(\varepsilon_0, \dot{\varepsilon}_0)$ plane. For the experimental data, open symbols correspond to fluidization, filled ones non-fluidization, and half-filled ones the critical condition. (a) The SC maneuver; (b) The CS and CH maneuvers. Model prediction at a lower $V_m = 0.025$ μm/s is also shown for comparison.

experiments fall within this portion ($\dot{\varepsilon} < 0.1$), and thus exhibit fluidization when either ε_0 or $\dot{\varepsilon}_0$ is high enough.

The critical conditions for compress-stretch (CS) and compress-hold (CH) maneuvers also present intriguing features (Fig. S1b). As the minimum tension (or largest compressive force) occurs during the compression phase of both CS and CH, the critical condition is the same for both maneuvers. Upon onset of compression, σ drops instantaneously to a local minimum thanks to the viscous force (cf. Fig. 3b). As σ falls below σ_0, the myosin apparatus starts to contract to alleviate the compression on the KV element, at a speed of $(m_1/m_t)V_m(1-\sigma/\sigma_0) = 0.533V_m(1-\sigma/\sigma_0)$ according to Eq. (6). Note that the equilibrium myosin ratio $m_1/m_t = 0.533$ holds as there has not been enough time for the myosin populations to evolve. Thus, for a small strain ε_0, the critical condition for fluidization amounts to $\sigma_{min} = GL_0\varepsilon_p - \eta(L_0\dot{\varepsilon}_0 - 0.533V_m) = 0$. We have ignored the elastic force due to compression because the strain ε_0 is small. This predicts a critical condition for small strain ε_0:

$$\dot{\varepsilon}_0 = 0.533\frac{V_m}{L_0} + \frac{G}{\eta}\varepsilon_p. \tag{1}$$

For a large strain, on the other hand, the critical condition of $\sigma = 0$ amounts to the myosin apparatus contracting at the zero-load speed of $0.714V_m$ (note

$m_1/m_t = 0.714$ at zero load), with the KV element completely relaxed. This gives a large-strain asymptote for the critical condition: $\dot{\varepsilon}_0 = 0.714 V_m/L_0$. Both limits are on the strain rate alone, regardless of the strain. Thus, for our parameters the model predicts a boundary that becomes flat at the left and right, with a negative slope in between. This is borne out in Fig. S1(b) by the boundaries at $V_m = 0.075$ and 0.025 μm/s; in each case, the small and large strain limits agree with the above estimations to within 1%.

2 Comparison with experiments

The critical condition for fluidization has been a focus of experimental investigations, and some of the data can be compared with our model predictions. So far, disassembly of stress fibers has been investigated under several type of mechanical perturbations: compress-hold (CH) (1, 2), stretch-compress (SC)(7, 8, 9), compress-stretch (CS) (9), and cyclic stretch (10, 11, 12, 13, 14, 15). Given sufficiently severe deformation (in terms of ε_0 or $\dot{\varepsilon}_0$), all these maneuvers have been shown to induce disassembly of stress fibers in the direction of compression.

Figure S1(a) compares the predicted critical condition for the SC maneuver with the experimental data of Chen et al. (9). Since the cyclic stretch amounts to repeated cycles of the SC maneuver, its critical $(\varepsilon_0, \dot{\varepsilon}_0)$ map should be essentially the same as that for the SC maneuver. Thus, we have included the cyclic-stretching data of Tondon et al. (15) and Kaunas et al. (10) as well. In these two data sets, we take the onset of SF alignment in the orthogonal direction as indicative of stress fiber disassembly in the stretching direction. First, note that all the data are for relatively small strain, $\dot{\varepsilon} \leq 0.1$, and thus cannot validate our prediction of a positive slope for larger strains. Within this range, the data do suggest a boundary corresponding to the critical condition that has a negative slope, as predicted by the model. Quantitatively, the predicted boundary is consistent with the only data point for SC (9), but is considerably higher than that suggested by the cyclic-stretch data.

Now we turn to the CS and CH maneuvers in Fig. S1(b). Again, the experimental data of Chen et al. (9) is consistent with the predicted critical condition; no fluidization occurs for $\varepsilon_0 = 0.1$ and $\dot{\varepsilon} = 0.05\ s^{-1}$, a condition below the theoretical curve. However, the CH experiments of Costa et al. (1) and Sato et al. (2) have reported buckling or disassembly of SFs at lower

strain rates of 0.02–0.03 s^{-1}. The data of Costa et al. (1) suggest a boundary with a negative slope, as predicted by the model, but the experimental boundary is much below the model prediction.

Comparing the experiments cited in Fig. S1 and similar ones in the literature, one may divide them into two groups according to substrate rigidity: experiments by Fredberg and colleagues (16, 7, 8, 9) have used very soft substrates, typically collagen and polyacrylamide gels, with a Young's modulus E up to 4 kPa, while all the other experiments (1, 2, 10, 15) have used much stiffer silicone-rubber substrates with E on the order of MPa. It is well known that substrate rigidity affects the cytoskeletal structure and mechanical behavior of adherent cells (17, 18). As we have used $V_m = 0.075$ μm/s in the model, a value matched to the excess tension in the soft-substrate experiment of Trepat et al. (16) (Fig. 7), it is reasonable that the predicted critical condition should agree with that of Chen et al. (9), another soft-substrate experiment. Stiffer substrates induce a larger number of stress fibers in the cell, larger traction forces and greater modulus of the whole cell (19, 20). In turn, these should affect the myosin concentration and sliding speed. Unfortunately, it is difficult to represent such effects in the model, say through Eq. (6), with any confidence. Assuming that the stiff substrates (1, 2, 10, 15) engender a stiffer myosin apparatus and slower myosin relaxation, we have computed the critical conditions for fluidization for a smaller characteristic $V_m = 0.025$ μm/s. Plotted as a dashed line in Fig. S1(b), the slower myosin relaxation does bring the model prediction closer to these stiff-substrate experiments for the CS and CH maneuvers.

To sum up the comparison above, the model prediction agrees qualitatively, and in some cases semi-quantitatively, with experimentally measured critical strains and strain rates for SF disassembly. Encouraging as it is, the agreement should be considered preliminary and perhaps tentative, in view of the uncertainty in the parameter V_m as well as the various assumptions that have gone into the model. These need to be investigated more thoroughly in future work.

Supporting References

(1) Costa, K. D., W. J. Hucker, and F. C. P. Yin, 2002. Buckling of actin stress fibers: a new wrinkle in the cytoskeletal tapestry. *Cell Motil. Cytoskel.* 52:266–274.

(2) Sato, K., T. Adachi, M. Matsuo, and Y. Tomita, 2005. Quantitative evaluation of threshold fiber strain that induces reorganization of cytoskeletal actin fiber structure in osteoblastic cells. *J. Biomech.* 38:1895–1901.

(3) Pirentis, A. P., E. Peruski, A. L. Iordan, and D. Stamenović, 2011. A Model for Stress Fiber Realignment Caused by Cytoskeletal Fluidization During Cyclic Stretching. *Cell. Mol. Bioeng.* 4:67–80.

(4) Soares e Silva, M., M. Depken, B. Stuhrmann, M. Korsten, F. C. MacKintosh, and G. H. Koenderink, 2011. Active multistage coarsening of actin networks driven by myosin motors. *Proc. Natl. Acad. Sci. USA* 108:9408.

(5) Veigel, C., J. E. Molloy, S. Schmitz, and K. Jones, 2003. Load-dependent kinetics of force production by smooth muscle myosin measured with optical tweezers. *Nat. Cell Biol.* 5:980–986.

(6) Kovács, M., K. Thirumurugan, P. J. Knight, and J. R. Sellers, 2007. Load-dependent mechanism of nonmuscle myosin 2. *Proc. Natl. Acad. Sci. USA* 104:9994–9999.

(7) Gavara, N., P. Roca-Cusachs, R. Sunyer, R. Farré, and D. Navajas, 2008. Mapping cell-matrix stresses during stretch reveals inelastic reorganization of the cytoskeleton. *Biophys. J.* 95:464–471.

(8) Krishnan, R., C. Y. Park, Y. C. Lin, J. Mead, R. T. Jaspers, X. Trepat, G. Lenormand, D. Tambe, A. V. Smolensky, A. H. Knoll, J. P. Butler, and J. J. Fredberg, 2009. Reinforcement versus fluidization in cytoskeletal mechanoresponsiveness. *PLoS One* 4:e5486.

(9) Chen, C., R. Krishnan, E. Zhou, A. Ramachandran, D. Tambe, K. Rajendran, R. M. Adam, L. Deng, and J. J. Fredberg, 2010. Fluidization and resolidification of the human bladder smooth muscle cell in response to transient stretch. *PLoS One* 5:e12035.

(10) Kaunas, R., P. Nguyen, S. Usami, and S. Chien, 2005. Cooperative effects of Rho and mechanical stretch on stress fiber organization. *Proc. Natl. Acad. Sci. USA* 102:15895–15900.

(11) Kaunas, R., and H.-J. Hsu, 2009. A kinematic model of stretch-induced stress fiber turnover and reorientation. *J. Theor. Biol.* 257:320–330.

(12) Hsu, H. J., C. F. Lee, A. Locke, S. Q. Vanderzyl, and R. Kaunas, 2010. Stretch-induced stress fiber remodeling and the activations JNK and ERK depend on mechanical strain rate, but not FAK. *PLoS One* 5:e12470.

(13) Kaunas, R., and S. Deguchi, 2011. Multiple roles for myosin II in tensional homeostasis under mechanical loading. *Cell. Mol. Bioeng.* 4:182–191.

(14) Kaunas, R., H.-J. Hsu, and S. Deguchi, 2011. Sarcomeric model of stretch-induced stress fiber reorganization. *Cell Health Cytoskel.* 3:13–22.

(15) Tondon, A., H.-J. Hsu, and R. Kaunas, 2012. Dependence of cyclic stretch-induced stress fiber reorientation on stretch waveform. *J. Biomech.* 45:728–735.

(16) Trepat, X., L. Deng, S. S. An, D. Navajas, D. J. Tschumperlin, W. T. Gerthoffer, J. P. Butler, and J. J. Fredberg, 2007. Universal physical responses to stretch in the living cell. *Nature* 447:592–595.

(17) Discher, D. E., P. A. Janmey, and Y.-L. Wang, 2005. Tissue cells feel and respond to the stiffness of their substrate. *Science* 310:1139–1143.

(18) Guo, W.-H., M. T. Frey, N. A. Burnham, and Y.-L. Wang, 2006. Substrate Rigidity Regulates the Formation and Maintenance of Tissues. *Biophys. J.* 90:2213–2220.

(19) Tee, S.-Y., J. Fu, C. S. Chen, and P. A. Janmey, 2011. Cell Shape and Substrate Rigidity Both Regulate Cell Stiffness. *Biophys. J.* 100:L25–L27.

(20) Jannat, R. A., M. Dembo, and D. A. Hammer, 2011. Traction Forces of Neutrophils Migrating on Compliant Substrates. *Biophys. J.* 101:575–584.